Interface optical phonon-assisted tunneling in double-barrier structures

Zu Wei Yan,[1,2,3,*] X. X. Liang,[1,2,†] and S. L. Ban[1,2]
[1]*CCAST (World Laboratory), P.O. Box 8730, Beijing 100080, People's Republic of China*
[2]*Department of Physics, Inner Mongolia University, Hohhot 010021, People's Republic of China*[‡]
[3]*Department of Basic Sciences, Inner Mongolia Agricultural University, Hohhot 010018, People's Republic of China*
(Received 30 March 2001; published 10 September 2001)

The phonon-assisted tunneling current in an asymmetric double-barrier structure is studied theoretically by considering the electron-interface optical-phonon interaction. The numerical results are obtained for the typical $Al_xGa_{1-x}As/GaAs/Al_yGa_{1-y}As$ structures and a new theoretical understanding about the experimental peaks of phonon-assisted tunneling current is proposed. It is found that only one phonon-assisted tunneling peak appears near the frequency of the well-longitudinal optical-phonon modes for the wider well case, and the contribution from the interface optical-phonon-assisted tunneling on the peak is dominant. The theory can explain the previous experimental results rationally.

DOI: 10.1103/PhysRevB.64.125321 PACS number(s): 73.40.Gk, 72.10.Di, 63.20.Kr

I. INTRODUCTION

The resonant tunneling (RT) in a double barrier structure (DBS)[1,2] is interesting to both scientific and technological researches. Several experiments at low temperature showed the additional satellite peaks in the current-voltage curve at an applied voltage locating just above the typical resonant peak. These peaks were attributed to the emission of longitudinal optical (LO) phonons by tunneling electrons.[3–5] Leadbeater *et al.* investigated the current-voltage characteristics of a series of $GaAs/Al_xGa_{1-x}As$ double-barrier structures in the presence of a magnetic-field perpendicular to the barriers.[3] The emission processes involving both the AlAs- and GaAs-like LO-phonon modes are observed for the narrower well cases (the well widths: 5 and 5.8 nm, but only one process emitting the GaAs-like phonons can be observed for a wider well (11.7 nm). Boebinger *et al.*[4] have observed the 2D magnetopolarons in a relatively narrow quantum well of 10 nm. It was also found that the second resonant tunneling-current peak assisted by AlAs (barrier) LO-phonon emission in the higher magnetic fields is much weaker than the first one. A possible explanation for the above phenomena is that the wave function of the quasibound state of electrons in the narrow GaAs quantum well penetrates easily into the $Al_xGa_{1-x}As$ barrier, so that tunneling electrons in narrower wells couple more effectively to the barrier-phonon modes. Even though there is not an absolute criterion for ''wide'' or ''narrow'' wells, the peak assisted by barrier phonons is, in a word, weaker and more difficult to be observed than the well-phonon one, even in narrower wells.

It is recognized that the interaction between the electrons and optical phonons in heterostructures is affected strongly by the presence of interfaces, which give rise to the appearance of the so-called interface-optical-(IO) phonon modes localized in the vicinities of the interfaces. Many theoretical and experimental physicists have studied the electron-phonon (e-p) interaction in layered materials and showed the importance of IO-modes for the physical properties of heterostructures.[6–12] Therefore at least two different types of phonon modes, the confined LO modes and IO modes, should be taken into account in consideration of the phonon-assisted tunneling (PAT) in DBS systems.

The LO-PAT in symmetric DBS's has been widely investigated theoretically.[13–17] Some authors[15–17] reported the theoretical works on the IO-PAT in symmetric DBS's Turley and Testsworth considered the so-called ''inner'' symmetric modes of IO phonons[15] as the most important IO modes in the PAT, which have the energies of bulk AlAs LO phonons in the long-wavelength limit. They asserted that the inner symmetric IO modes contribute to the second peak in the experiments. In view of above-mentioned analysis, the two PAT peaks are attributed, respectively, to the confined GaAs LO phonons in the well and the IO phonons with AlAs LO frequency even for the wider quantum-well cases. Moreover, a stronger current peak assisted by the IO-phonon modes of AlAs LO frequency than that by the GaAs LO-phonon modes is obtained. Unfortunately, the theoretical results cannot match entirely the experimental observations. As mentioned above, the second peak in the experiments is found much weaker than the first peak and the PAT currents are sensitive to the well width of the DBS. Only one PAT peak can be easily observed when the well is wider, but the second peak appears as the well width becomes narrower.[3,4] Judging from this a theoretical rerecognition for the experimental peaks of PAT currents is need.

Furthermore, the experimental investigations indicate that the asymmetric DBS (ADBS) may vary the charge accumulation in the well so that the current-voltage characteristics can be modified and the resonant current peaks are enhanced.[18–20] However, few theoretical results about the IO-phonon contributions to the PAT in an ADBS have been reported, to our knowledge. Therefore, theoretical investigations in detail for the IO-phonon effects on the RT in an ADBS are invoked.

In this paper, we calculate the phonon emission rate and the PAT current in an ADBS, by including all the branches of IO-phonon modes besides the LO phonons. We first derive the expressions for the phonon modes and the e-p coupling functions within the framework of the dielectric continuum model in Sec. II. The phonon-emission rate and the PAT current for both LO- and IO-phonon modes in an ADBS are calculated in Sec. III. The numerical computations have been performed for several ADBS systems and the results are illustrated and discussed in Sec. IV. The properties of the pho-

non modes and the e-p coupling for all the eight branches of IO modes are analyzed. By comparing the e-p coupling strengths with phonon-emission rates, the most important branch of IO modes is determined different from the previous theoretical works.[15,16] The PAT currents including the contributions of total eight branches of IO modes are numerically obtained for different ADBS systems. Different from the previous points,[10–12] our results show that the IO phonons with the energy of the bulk GaAs LO phonons, instead of that with the bulk AlAs LO phonons, are most important in the electron-IO-phonon (e-IO-p) couplings. A new understanding for the experimental results[3,4] is proposed based on the theoretical calculations. Theoretical results indicate that the PAT peaks from both IO phonons and confined well LO phonons occur at the same frequency of the bulk GaAs LO-phonons and merge to be single one. The IO-phonon contributions are more significant than that from the LO phonons confined in the well and barriers. Only one PAT peak (corresponding to the GaAs LO-like phonon energy) is easily observed in the wider well ADBS.

II. ELECTRON-PHONON INTERACTION HAMILTONIAN

Consider a DBS composed of five layers of polar crystals labeled by 1, 2, 3, 4, and 5 and located in region I ($z<-d_2-d_3/2$), II ($-d_2-d_3/2\leqslant z<-d_3/2$), III ($-d_3/2\leqslant z<d_3/2$), IV ($d_3/2\leqslant z<d_4+d_3/2$), and V ($z\geqslant d_4+d_3/2$), respectively. Within the framework of the dielectric-continuum model, electrostatic potential $\Phi(\mathbf{r})$ satisfies the following equation:

$$\varepsilon_j(\omega)\nabla^2\Phi(\mathbf{r})=0, \tag{1}$$

where

$$\varepsilon_j(\omega)=\varepsilon_{\infty j}\frac{\omega^2-\omega_{Lj}^2}{\omega^2-\omega_{Tj}^2}, \tag{2}$$

$\varepsilon_j(\omega)$ and $(\varepsilon_{\infty j})$ are the frequency-dependent and high-frequency dielectric constants, respectively. ω_{Lj} and ω_{Tj} are, respectively, the LO and transverse optical (TO) phonon frequencies in layer "j." The electrostatic boundary condition requires that both $\Phi(\mathbf{r})$ and the z component of the electric displacement $D_z=-\varepsilon_j(\omega)(\partial\Phi/\partial z)$ remain continuous across the interfaces.

In consideration of the translation invariance in the x-y plane, we expand the electrostatic potential due to the phonons as follows:

$$\Phi(\mathbf{r})=\sum_{\mathbf{q}}\frac{1}{\sqrt{S}}\xi(\mathbf{q})f(q,z)e^{i\mathbf{q}\cdot\boldsymbol{\rho}}, \tag{3}$$

where S is the area of the interfaces, $\mathbf{q}$ and $\boldsymbol{\rho}$ are, respectively, the two-dimensional wave vector and position vector in the x-y plane.

Solving Eq. (1) with the boundary condition gives two kinds of polarization modes. The confined LO modes have been given in the previous papers[9–11] and their detailed forms are neglected here.

The dispersion relation of IO phonons is then obtained as

$$r_2r_4+g_2g_4e^{-2qd_3}=0, \tag{4}$$

where

$$\begin{aligned}
r_2&=(\varepsilon_2+\varepsilon_1)(\varepsilon_3+\varepsilon_2)+(\varepsilon_2-\varepsilon_1)(\varepsilon_3-\varepsilon_2)e^{-2qd_2},\\
g_2&=(\varepsilon_2+\varepsilon_1)(\varepsilon_3-\varepsilon_2)+(\varepsilon_2-\varepsilon_1)(\varepsilon_3+\varepsilon_2)e^{-2qd_2},\\
r_4&=(\varepsilon_4+\varepsilon_3)(\varepsilon_5+\varepsilon_4)+(\varepsilon_4-\varepsilon_3)(\varepsilon_5-\varepsilon_4)e^{-2qd_4},\\
g_4&=(\varepsilon_4-\varepsilon_3)(\varepsilon_5+\varepsilon_4)+(\varepsilon_4+\varepsilon_3)(\varepsilon_5-\varepsilon_4)e^{-2qd4}.
\end{aligned} \tag{5}$$

Inserting Eq. (2) into Eq. (4), one can obtain an eighth-order equation for ω. There are, in principle, eight branches of frequencies denoted as $\omega_\nu(q)$ ($\nu=1,2,3,4,5,6,7,8$) as functions of wave vector q. The eigensolution of the IO-phonon potential in the DBS can be written as

$$f(q,z)=C\begin{cases} b_1e^{qz}, & z<-d_z-d_3/2\\ a_2e^{-qz}+b_2e^{qz}, & -d_2-d_3/2\leqslant z<-d_3/2\\ a_3e^{-qz}+e^{qz}, & -d_3/2\leqslant z<d_3/2\\ a_4e^{-qz}+b_4e^{qz}, & d_3/2\leqslant z<d_4+d_3/2\\ a_5e^{-qz}, & z\geqslant d_4+d_3/2, \end{cases} \tag{6}$$

where C is the normalization constant and satisfies

$$C=\left(\sum_{j=1}^{5}\eta_j\right)^{-1/2}, \tag{7}$$

with

$$\begin{aligned}
\eta_1&=\frac{b_1^2}{2q}\exp[-2q(d_2+d_3/2)],\\
\eta_2&=\frac{\sinh qd_2}{q}(a_2^2e^{q(d_2+d_3)}+b_2^2e^{-q(d_2+d_3)})+2a_2b_2d_2,\\
\eta_3&=\frac{\sinh qd_3}{q}(a_3^2+1)+2a_3d_3,\\
\eta_4&=\frac{\sinh qd_4}{q}(a_4^2e^{-q(d_3+d_4)}+b_4^2e^{q(d_3+d_4)})+2a_4b_4d_4,\\
\eta_5&=\frac{a_5^2}{2q}\exp[-2q(d_4+d_3/2)].
\end{aligned} \tag{8a}$$

The coefficients in Eqs. (6) and (8a) are given by

$$\begin{aligned}
a_2&=\frac{2\varepsilon_3}{r_2}(\varepsilon_2-\varepsilon_1)e^{-2q(d_2+d_3/2)},\quad a_3=\frac{g_2}{r_2}e^{-qd_3},\\
a_4&=\frac{1}{2\varepsilon_4r_2}[(\varepsilon_4+\varepsilon_3)g_2e^{-qd_3}+(\varepsilon_4-\varepsilon_3)r_2e^{qd_3}],\\
a_5&=\frac{1}{(\varepsilon_5+\varepsilon_4)r_2}[(\varepsilon_4+\varepsilon_3)g_2e^{-qd_3}+(\varepsilon_4-\varepsilon_3)r_2e^{qd_3}],
\end{aligned} \tag{8b}$$

$$b_1=\frac{4\varepsilon_2\varepsilon_3}{r_2},\quad b_2=\frac{2\varepsilon_3}{r_2}(\varepsilon_2+\varepsilon_1),$$

$$b_4=\frac{1}{2\varepsilon_4 r_2}[(\varepsilon_4-\varepsilon_3)g_2e^{-2qd_3}+(\varepsilon_4+\varepsilon_3)r_2].$$

Finally, we can write the electron-phonon (e-p) interaction Hamiltonian as

$$H_{e\text{-}p}=H_{e\text{-LO}}+H_{e\text{-IO}}, \tag{9}$$

where $H_{e\text{-LO}}$ and $H_{e\text{-IO}}$ describe the e-LO-p and e-IO-p interactions, respectively. The e-IO-p interaction Hamiltonian can be written as

$$H_{e\text{-IO}}=\sum_{\mathbf{q}\nu}\frac{1}{\sqrt{S}}\beta_\nu(q)f_\nu(q,z)e^{i\mathbf{q}\cdot\boldsymbol{\rho}}a_{\mathbf{q}\nu}+\text{H.c.}, \tag{10}$$

where $a_{\mathbf{q}}$ and $a_{\mathbf{q}}^+$ are, respectively, the annihilation and creation operators for the phonons, and the coupling function $\beta_\nu(q)$ is given by

$$\beta_\nu(q)=\left(\frac{e^2\hbar}{\varepsilon_0 q}\right)^{1/2}\left(C^2\sum_{j=1}^{5}I_{j\nu}\right)^{-1/2}, \tag{11}$$

with

$$I_{1\nu}=b_1^2\left(\frac{\partial\varepsilon_1}{\partial\omega}\right)_\nu\exp[-2q(d_2+d_3/2)],$$

$$I_{2\nu}=2\sinh(qd_2)\left(\frac{\partial\varepsilon_2}{\partial\omega}\right)_\nu(a_2^2e^{q(d_2+d_3)}+b_2^2e^{-q(d_2+d_3)}),$$

$$I_{3\nu}=2\sinh(qd_3)\left(\frac{\partial\varepsilon_3}{\partial\omega}\right)(a_3^2+1),$$

$$I_{4\nu}=2\sinh(qd_4)\left(\frac{\partial\varepsilon_4}{\partial\omega}\right)_\nu(a_4^2e^{-q(d_3+d_4)}+b_4^2e^{q(d_3+d_4)}), \tag{12}$$

$$I_{5\nu}=a_5^2\left(\frac{\partial\varepsilon_5}{\partial\omega}\right)_\nu\exp[-2q(d_4+d_3/2)],$$

$$\text{and}\quad\left(\frac{\partial\varepsilon_j}{\partial\omega}\right)_\nu=2\varepsilon_{\infty j}\omega_\nu\frac{\omega_{lj}^2-\omega_{Tj}^2}{\omega_\nu^2-\omega_{Tj}^2},\quad j=1,2,3,4,5.$$

III. PHONON-ASSISTED TUNNELING CURRENT

We consider a PAT process in which an electron with energy E is incident into an ADBS system under an applied voltage. The potential influencing the electron varies only in the z direction. The wave function associated with the bare electron can be written as

$$\Psi(\mathbf{r})=\frac{1}{\sqrt{S}}e^{i\boldsymbol{\rho}\cdot\mathbf{k}_t}\varphi(z), \tag{13}$$

where $\boldsymbol{\rho}$ and $\mathbf{k}_t$, are, respectively, the position and wave vector projected onto the interface plane. $\mathbf{k}=(\mathbf{k}_t,\mathbf{k}_z)$ is the total wave vector. Here the effective-mass approximation has been used and the effect of kinetic-energy confinement is neglected. $\varphi(z)$ will be determined numerically by solving a 1D Schrödinger equation in the z direction[21]

$$-\frac{\hbar^2}{2}\frac{d}{dz}\left[\frac{1}{m^*(z)}\right]\frac{d\varphi}{dz}+U(z)\varphi(z)=E_z\varphi(z), \tag{14}$$

where $m^*(z)$ denotes the position-dependent electron-band mass and $U(z)$ the potential. Then the electron energy E can be written as the sum of the parallel and transverse components,

$$E=\frac{\hbar^2k_t^2}{2m^*}+E_z. \tag{15}$$

The emitter electronic wave function extends into the DBS with the emission of optical phonons. The phonon emission rates in the system can be obtained by the usual Fermi golden rules

$$W^{i\to f}(\mathbf{k})=\frac{2\pi}{\hbar}|\langle f|H_{e\text{-}ph}|i\rangle|^2\delta(E_i-E_f-\hbar\omega(q)), \tag{16}$$

where E_i and E_j denote the energies of the initial and final electronic states. The initial and final states are, respectively, the single-electronic states without phonons and with an emitted phonon, which can be given by

$$\begin{aligned}|i\rangle&=|\psi_i\rangle|0_q\rangle,\\ |f\rangle&=|\psi_f\rangle|1_q\rangle,\end{aligned} \tag{17}$$

where $|0_q\rangle$ and $|l_q\rangle$ are, respectively, the states of zero phonon and one phonon with wave vector q. The emitted phonon energies $\hbar\omega(q)$ are, respectively, chosen as $\hbar\omega_{\text{LO}}$ for the confined LO phonons and $\hbar\omega_{\text{IO}}(q)$ for the IO phonons in the calculations.

Substituting Eqs. (13) and (17) and $H_{e\text{-IO}}$ into Eq. (16), the emission rate is given by

$$W^{t\to f}(\mathbf{k}_i,\mathbf{k}_f)=\frac{2\pi}{S\hbar}\beta^2(q)|M(q)|^2\delta_{\mathbf{k}_n-\mathbf{k}_{tf}-\mathbf{q}}\times\delta(E_i-E_f-\hbar\omega(q)), \tag{18}$$

where $M(q)$ is the overlap integral,

$$M(q)=\int_{-\infty}^{\infty}\varphi_f^*(z)f(q,z)\varphi_i(z)dz. \tag{19}$$

Summing the emission rate (18) over all allowable final states (in fact over the phonon wave vector $\mathbf{q}$), one can obtain the total emission rate from $|i\rangle$ to $|f\rangle$,

$$W(\mathbf{k},V)=\sum_{\mathbf{q}}W^{i\to f}(\mathbf{k},\mathbf{q}), \tag{20}$$

which is a function of wave vector $\mathbf{k}$ and applied voltage V.

TABLE I. Parameters used in the numerical calculation. Energy is in units of meV and mass is in units of the bare electron mass.

Quantities	GaAs	$Al_xGa_{1-x}As$
m	0.067	$0.067+0.083x$
$\hbar\omega_{LO}$	36.25	$36.25+1.83x+17.12x^2-5.11x^3$
$\hbar\omega_{TO}$	33.29	$33.29+10.70x+0.03x^2+0.086x^3$
ε_0	13.18	$13.18-3.12x$
ε_∞	10.89	$10.89-2.73x$

The condition of energy conservation $E_t-E_f-\hbar\omega(q)=0$ in this process can be rewritten as

$$k_{ti}^2-k_{tf}^2-\frac{2m^*}{\hbar^2}[\hbar\omega(q)-\Delta E_z]=0, \tag{21}$$

where $\Delta E_z=E_{zi}-E_{zf}$ is the energy loss in the z direction. Inserting the conservation of momentum $\mathbf{k}_{ti}-\mathbf{k}_{tf}-\mathbf{q}=0$ into Eq. (21), we have

$$q^2-2k_{ti}q\cos\theta+\frac{2m^*}{\hbar^2}[\hbar\omega(q)-\Delta E_z]=0. \tag{22}$$

Here θ is the angle between the wave vectors of the incident electron and the emitted phonon in the x-y plane. Transforming the summation in Eq. (20) into an integral, the phonon emission rate can be written as

$$W(\mathbf{k},V)=\frac{m^*}{\pi\hbar^3}\sum_l\int_0^{\theta_{\max}}d\theta \times\frac{\beta^2(q_l)|M(q_l)|^2q_l}{\left|q_l-k_{ti}\cos\theta+\frac{m^*}{\hbar}\left(\frac{\partial\omega(q)}{\partial q}\right)_{q=q_l}\right|}, \tag{23}$$

where $\theta_{\max}$ is the maximum scattering angle. Moreover the voltage dependence of the emission rate due to $M(q_l)$ and q_l must satisfy Eq. (22).

In the long-wavelength limit, $\hbar\omega(q)=\hbar\omega=$const and $\partial\omega(q)/\partial q=0$. For $\hbar\omega-\hbar^2k_{ti}^2/2m^*\leqslant\Delta E_z<\hbar\omega$, Eq. (23) can be simply written as

$$W(\mathbf{k},V)=\frac{2m^*}{\pi\hbar^3}\int_0^{\theta_{\max}}d\theta \times\frac{\beta^2(q_1)|M(q_1)|^2q_1+\beta^2(q_2)|M(q_2)|^2q_2}{|q_1-q_2|}, \tag{24}$$

where

$$q_{1,2}=k_{ti}\cos\theta\pm\sqrt{(k_{ti}\cos\theta)^2-\frac{2m^*}{\hbar^2}(\hbar\omega-\Delta E_z)}, \tag{25}$$

$$\theta_{\max}=\cos^{-1}\sqrt{\frac{2m^*}{\hbar^2}(\hbar\omega-\Delta E_z)}. \tag{26}$$

For $\Delta E_z\geqslant\hbar\omega$,

$$W(\mathbf{k},V)=\frac{2m^*}{\pi\hbar^3}\int_0^{\pi}d\theta\frac{\beta^2(q_1)|M(q_1)|^2q_1}{|q_1-q_2|}. \tag{27}$$

The total excess current density due to IO-phonon-assisted tunneling can be calculated by

$$J(V)=\frac{e}{S}\sum_{\nu=1}^{8}\int W(\mathbf{k},V)g(\mathbf{k})f(\mathbf{k})d\mathbf{k}, \tag{28}$$

where $f(\mathbf{k})$ and $g(\mathbf{k})=2SL/(2\pi)^3$ are, respectively, the Fermi function and the electron state density of the emitter. SL is the emitter effective volume. We focus our discussion on the low-temperature case and then the phonon-absorption effects can be neglected in Eq. (28). It is also assumed that the tunneling current is small enough so that the electron state occupation and the phonon population are in equilibrium states. Thus, the current density can be calculated by

$$J(V)=\frac{em^{*3/2}L}{2^{3/2}\pi^2\hbar^3}\sum_{\nu=1}^{8}\int_0^{\infty}dE_z\int_0^{\infty}\frac{W(E,V)f(E)}{\sqrt{E_z}}dE_t, \tag{29}$$

$$\text{where}\quad f(E)=\frac{1}{e^{(E-E_F)/k_BT}+1}.$$

Here E_F is the Fermi energy, T is the temperature, and k_B is the Boltzmann constant.

An analogous formula can be also derived for the confined LO-PAT currents in the well and the barriers and is simpler than that for the IO PAT. For the sake of simplification, we do not list them here.

IV. NUMERICAL RESULTS AND DISCUSSION

By using the analytical expressions for the optical phonon modes, the e-p interaction Hamiltonian, phonon-emission rate, and the phonon-assisted current given above, we have performed the numerical calculations for a typical ADBS $GaAs/Al_{0.35}Ga_{0.65}As/GaAs/Al_{0.4}Ga_{0.6}As/GaAs$ system with corresponding widths of $-\infty$/20 Å/50 Å/25 Å/∞. The potential-barrier height of the $Al_xGa_{1-x}As$ is determined by $V(x)=750x$ (meV) for $x\leqslant0.45$ and $V(x)=750x+690(x-0.45)^2$ (meV) for $0.45\leqslant x\leqslant1$.[21] An external electric voltage is applied in the z direction. The parameters used in the computation are listed in Table I (Ref. 22) and the results are illustrated in Figs. 1–8.

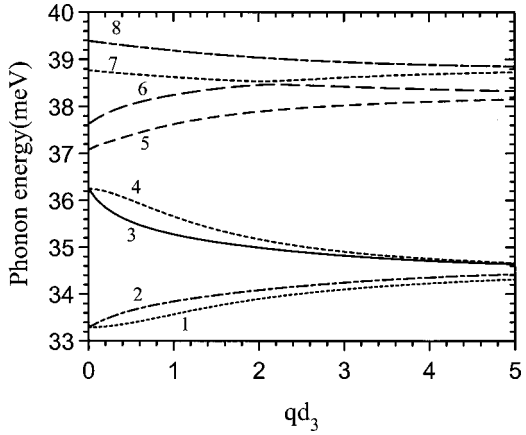

FIG. 1. IO-phonon energies $\hbar\omega_\nu$ as functions of wave vector q. Curves are labeled from lower to higher energies.

Figure 1 gives the dispersion relations of the IO-phonon modes as functions of qd_3. It is clearly seen that there are eight branches of frequency solutions for the IO-phonon modes (labeled from lower to higher frequencies). As pointed out in a previous paper,[10] every interface between two different media gives rise to two branches of IO-phonon modes. It can be found from Fig. 1 that the eight frequency branches can be divided into two groups. The phonon energies of the four branches with lower frequencies distribute in the range from 33.29 to 36.25 meV at $q\rightarrow 0$, corresponding, respectively, to the bulk TO and LO frequencies in GaAs and hereafter we name them GaAs-like branches for convenience. The other four branches locating in the range between 37 and 39.39 meV at $q\rightarrow 0$ can be named as $Al_xGa_{1-x}As$-like branches. It is easily understood that all the IO-phonon modes interact with the electron, although their coupling strengths are obviously different.

The phonon potentials $f(q,z)$ of the eight branches of the IO modes are plotted as functions of z with $qd_3=1$ in Fig. 2. It is shown that the phonon potentials reach their peaks at the interfaces, and are mainly localized in the vicinity of the interfaces, respectively. It is noteworthy that branch 3 of the IO phonon modes (the solid line in Fig. 2) with the bulk GaAs LO-phonon energy (36.25 meV) at $q\rightarrow 0$ is localized

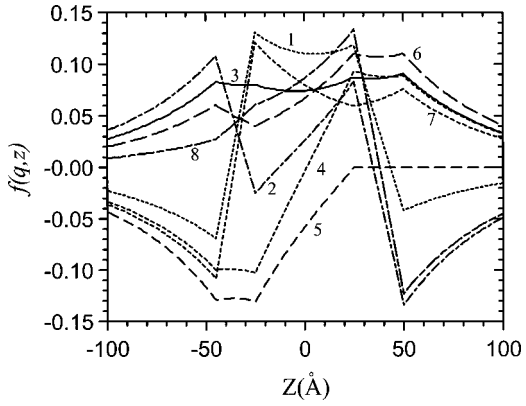

FIG. 2. IO-phonon potentials as functions of z with $qd_3=1$. Curves labeled from 1 to 8 correspond to Fig. 1.

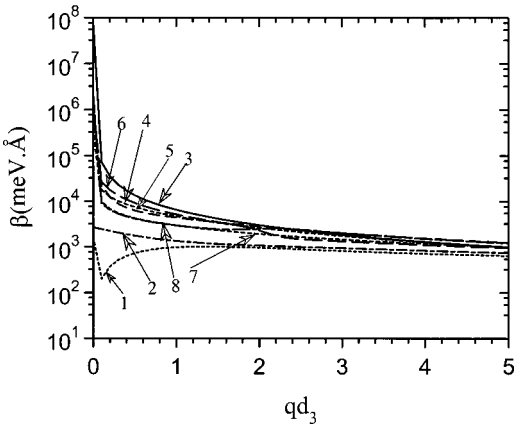

FIG. 3. The coupling coefficient $\beta(q)$ as a function of wave vector q on a logarithmic scale. Curves labeled from 1 to 8 correspond to Fig. 1.

mainly in the vicinities of the interfaces at $z=-d_2-d_3/2=-45$ Å and $z=d_4+d_3/2=50$ Å. It is nearly symmetric with respect to the center of the ADBS and has quite a good behavior of propagation in the system.

Figure 3 shows the e-IO-p interaction coupling functions $\beta(q)$ as functions of qd_3. It is easily seen that the values of $\beta(q)$ for branches 3–8 are much larger than that for branches 1,2 when $q\rightarrow 0$. It should be pointed out that $\beta(q)$ for branch 3 is largest in the long-wavelength limit. Meanwhile, $\beta(q)$ for branch 1 with the bulk GaAs TO-phonon energy (33.3 meV) is smallest in the eight branches of the IO modes. In the limit of $q\rightarrow\infty$, the eight branches of coupling functions tend to the same order of magnitude.

As pointed out above, the easy propagation property of branch 3 gives rise to a small peak-to-valley ratio of its mode amplitudes in the entire structure. In other words, this mode easily couples with the electrons. Thus the corresponding e-IO-p coupling function $\beta(q)$ for this mode is strongest in the ADBS. It can be seen from Eqs. (18), (19), and (29) that larger the $f(q,z)$ and $\beta(q)$, the bigger the contribution to the PAT current from the e-p interaction.

In Fig. 4, the phonon-emission rates of the eight branches

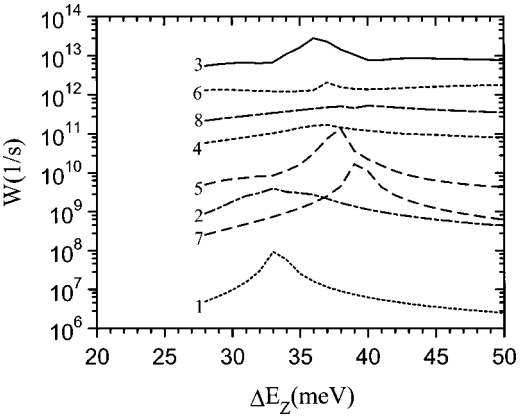

FIG. 4. The IO-phonon emission rate as a function of energy-level separation ΔE_z and the fixed applied voltage $V=200$ mV on a logarithmic scale. Curves labeled from 1 to 8 correspond to Fig. 1.

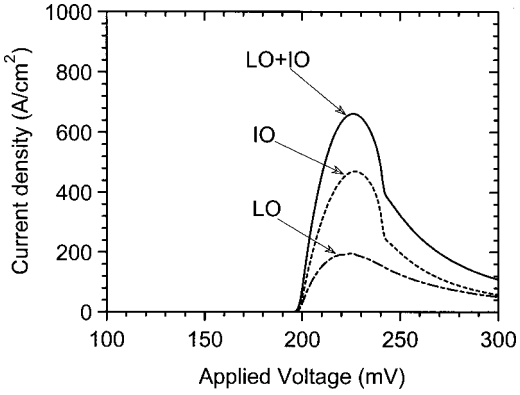

FIG. 5. The PAT current as a function of the applied voltage V with Femi energy $E_F=20$ meV and temperature $T=4$ K.

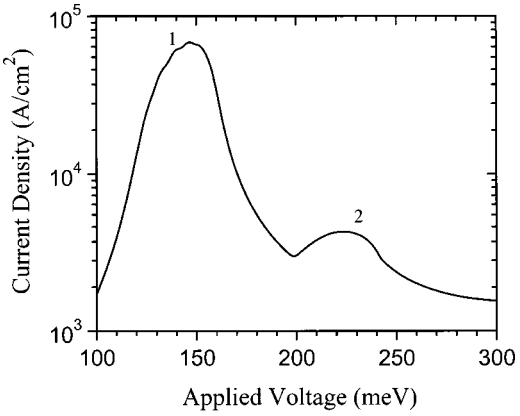

FIG. 6. The RT current as a function of applied voltage V on a logarithmic scale with Femi energy $E_F=20$ meV and temperature $T=4$ K: 1 denotes the RT current main peak and 2 denotes the PAT current peak.

of IO-modes are plotted as functions of ΔE_z for the fixed applied voltage $V=200$ mV. In the calculations wave functions $\varphi_i(z)$ and $\varphi_f(z)$ are numerically determined by a standard transfer-matrix method.[21] They have been normalized in the whole region of the ADBS including the emitter and collector. Here we have taken φ_i to be a plane wave in the emitter region, and φ_f the quasibound resonant wave function with energy E_{zf}. As was seen in Fig. 3, the contributions of the e-IO-p coupling in the vicinity of $q=0$ are dominant for all the eight branches of IO modes. Hence the frequencies of the emitted IO phonons are chosen as the corresponding values at the long-wavelength limit ($q\rightarrow 0$) for the sake of calculating easily. It is seen in Fig. 4 that the peaks of the eight emission-rate curves occur at different $\Delta E_z(=\hbar\omega_\nu)$ and have the differences of magnitude for the different branches of IO phonons. The branch 3 gives the largest contribution to the IO-phonon emission rate and is then dominant in the IO-phonon-assisted tunneling processes. This result can be understood from two respects: Firstly, the e-IO-p interaction from branch 3 is strongest in the eight branches of IO modes. Secondly, the phonon potential $f(q,z)$ of branch 3 is higher in the (wide) well and almost symmetric for the ADBS system and the resonant electronic state wave function $\varphi(z)$ is approximately localized in the GaAs well, so that the corresponding matrix element $M(q)$ in Eq. (19) is also larger.

Figure 5 illustrates the tunneling current densities assisted by the confined LO and total IO phonons as functions of the applied voltage at temperature 4 K. As expected, the IO-PAT current peak occurs at the voltage corresponding to the frequency of branch 3 at $q\rightarrow 0$, i.e., the GaAs LO frequency, since the contribution from the other seven branches of IO modes is stifled (see Fig. 4). It is interesting that the peaks of the confined LO- and IO-phonon-assisted currents occur at the same applied voltage near the vicinity of 220 mV.

Only one PAT current peak at the phonon energy around 35 meV, which is slightly lower than the LO-phonon energy of GaAs well, has been observed[3,4] for the wider quantum-well system. This deviation from LO-phonon energy can be understood by our theoretical results. In the calculation of the IO-PAT current, the phonon frequencies, in general, are chosen as the dispersionless frequencies at the long-wavelength limit ($q\rightarrow 0$). The IO frequency of the dominant branch of IO-phonon modes, i.e., branch 3, has been chosen as the LO frequency of GaAs, 36.25 meV. In fact, the frequencies of IO-phonon modes depend on their wave vectors. The phonon energy of branch 3 decreases and becomes lower than that of LO phonons by increasing the wave vector (Fig. 1). The emitted IO phonons of $q\neq 0$ have the energies smaller than 36.25 meV so that the peak of the phonon emission rate would be lowered if one takes the IO-phonon frequency dispersion into account. The corrected theoretical peak of the PAT current should reasonably appear at the energy lower than the LO-phonon energy of GaAs. To sum up, we recognize that the single-PAT peak is attributed to both IO and LO phonons in the well.

Figure 6 shows the contribution of the main RT and the PAT (including both confined LO and IO phonons) to the current density as functions of the applied voltage V for the ADBS same as above. In the calculations we have used the Tsu-Esaki current formula,[16] and chosen $E_F=20$ meV (corresponding to a doping of roughly 2×10^{17} cm^{-3} in the emitter layer) and $T=4$ K. The peaks for the RT and PAT currents, respectively, occur approximately at 140 and 220 mV. The calculated relative intensity of the PAT current peak here is given as 5.2%. The corresponding experimental result given by Goldman, Tsui, and Gunningham[23] is around 4% for a symmetric system. It may be seen that our theoretical results are in agreement with the experimental data.

Figure 7 illustrates the PAT current curves for the ADBS's with different Al composition y of the collector barriers, which can adjust the heights of collector barriers. The structure of the system in the calculation is chosen as $Al_{0.35}Ga_{0.65}As/GaAs/Al_yGa_{1-y}As$ with widths of 20 Å/50 Å/20 Å. It can be seen that the asymmetry of the structures may modulate the PAT current, by regulating the heights and the widths of the barriers of the asymmetric structures. The PAT peak becomes higher and easy to be observed as the collector barrier is heightened due to quantum-coherence effect. This makes the asymmetric structures more often applied in practical devices. It is seen that our model can be easily extended to the symmetric DBS case.

It was experimentally verified that the well width of the

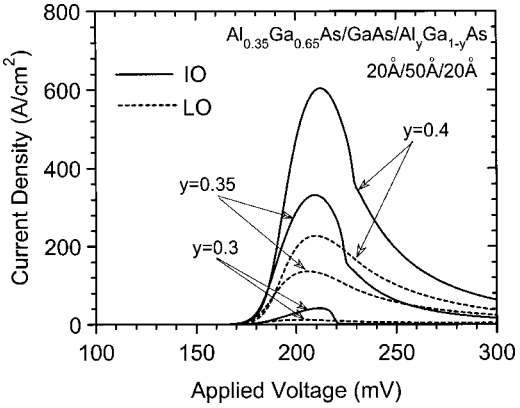

FIG. 7. PAT-current peaks versus the potential height of collector barrier for the $Al_{0.35}Ga_{0.65}As/GaAs/Al_yGa_{1-y}As$ structure with the widths of 20 Å/50 Å/20 Å.

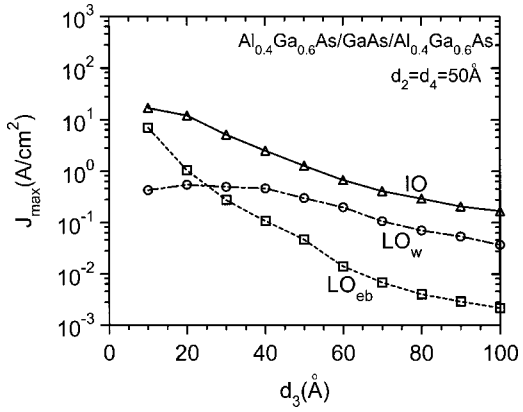

FIG. 8. The total IO-PAT current (solid line), the LO_w-PAT current (dash-dot line), and the LO_{eb}-PAT current (dash line) as functions of well width d_3 for the $Al_{0.4}Ga_{0.6}As/GaAs/Al_{0.4}Ga_{0.6}As$ structure with two barrier widths $d_2 = 50$ Å and $d_4 = 50$ Å.

DBS is an important factor for the PAT current peaks. Only one PAT peak has been easily observed when the well is wider, but the second peak appears as the well becomes narrower.[3,4] To investigate theoretically the dependence of the IO- and confined LO-PAT currents on the well width, we have calculated the PAT currents contributed by the IO phonon, the confined LO_w phonon (in well), and the confined LO_{eb} phonon (in emitter barrier), respectively, as functions of the well width d_3. In our computation the structures have been chosen as the symmetric DBS $Al_{0.4}Ga_{0.6}As/GaAs/Al_{0.4}Ga_{0.6}As$ with two barrier widths $d_2 = d_4 = 50$ Å. The results for the IO-, LO_w-, and LO_{eb}-PAT peaks are illustrated in Fig. 8. It can be seen that the peaks corresponding to the total IO phonon and two branches of LO phonons (LO_w and LO_{eb}) increase as the well-width narrowing. The IO-PAT peak is much more important than confined LO_w- and LO_{eb}-PAT peaks and the LO_w-PAT peak is much higher than the LO_{eb}-PAT peak when the well is wider. As a result, the LO_{eb}-PAT current is covered up by the LO_w-PAT current and only the first peak corresponding to the emission of confined LO_w phonons in the well and IO phonons (both with the energy of bulk GaAs LO-phonon) can easily be observed for the wider-well systems. It is also noticed that the LO_w-PAT peak grows in comparison with the IO-PAT peak when the well width becomes wider. With reducing the well width, the LO_{eb}-PAT peak rapidly increases and finally becomes much higher than the LO_w-PAT peaks so that the second peak corresponding to the emission of confined LO_{eb} phonons in the barrier can be observed. The intersection between the LO_{eb}-PAT and LO_w-PAT peaks occurs at $d_3 \approx 25$ Å, which is approximately one-half of the barrier width. It is also seen from our results that the second peak is much weaker than the first. Different from the previous references,[15,16] our theoretical results can qualitatively explain the above-mentioned experimental phenomena.[3,4]

In summary, we have generally calculated the e-p interactions in an arbitrary DBS based on the macroscopic dielectric continuum model. The phonon-emission rates and phonon-assisted currents have been investigated in detail for the DBS to verify the effects of the different phonon modes. The numerical computation is performed for the $GaAs/Al_{0.35}Ga_{0.65}As/GaAs/Al_{0.4}Ga_{0.6}As/GaAs$ system with the thickness $-\infty$/20 Å/50 Å/25 Å/∞. It is found that only one PAT peak can be observed for the wider-well case, which is contributed from the IO phonons with the LO-phonon energy of the GaAs well and the confined LO phonons in the well. It also can be seen that the IO PAT is much more important than the confined LO phonon. The dependence of the PAT currents on the potential height of collector barrier and well widths is discussed. It follows that the second PAT peak appears when the well is very narrow. Our recognition of the PAT-current peaks is different from the previous theoretical explanations[15,16] and agrees with the experimental results. It is to be pointed out that the more complicated electron-electron interaction is ignored in our discussion to focus the attention on the PAT processes. This effect will be discussed in the further work.

ACKNOWLEDGMENTS

The work was supported by the National Natural Science Foundation of China (Project No. 19764001) and the Natural Science Foundation and the 321 project of the Inner Mongolia Autonomous Region of China and the China Scholarship Council.

*Email address: zuweiyan@263.net
†Email address: xxliang@imu.edu.cn
‡Mailing address.

[1] L. L. Chang, L. Esaki, and R. Tsu, Appl. Phys. Lett. **24**, 593 (1974).
[2] F. Capasso and S. Datta, Phys. Today **43**, 74 (1990).
[3] M. L. Leadbeater, E. S. Alves, L. Eaves, M. Henini, O. H. Hughes, A. Celeste, J. C. Portal, G. Hill, and M. A. Pate, Phys. Rev. B **39**, 3438 (1989).
[4] G. S. Boebinger, A. F. J. Levi, S. Schmitt-Pink, A. Passner, L. N.

Pfeiffer, and K. W. West, Phys. Rev. Lett. **65**, 235 (1990).
[5] M. V. Petrov, S. P. Parichar, and S. A. Lyon, Phys. Rev. B **54**, 13 868 (1996).
[6] M. Ziesmann, D. Heitmann, and L. L. Chang, Phys. Rev. B **35**, 4541 (1987).
[7] M. A. Brummell, R. J. Nicholas, M. A. Hopkins, J. J. Harris, and C. T. Foxon, Phys. Rev. Lett. **58**, 77 (1987).
[8] K. Huang and B. Zhu, Phys. Rev. B **38**, 13 377 (1988).
[9] N. Mori and T. Ando, Phys. Rev. B **40**, 6175 (1989).
[10] X. X. Liang and S. G. Davison, Surf. Sci. **298**, 225 (1993).
[11] X. X. Liang, J. Phys.: Condens. Matter **4**, 9769 (1992).
[12] H. Rucker, E. Molinari, and P. Lugli, Phys. Rev. B **44**, 3463 (1991).
[13] N. S. Wingreen, K. W. Jacobsen, and J. W. Wilkins, Phys. Rev. B **40**, 11 834 (1989).
[14] F. Chevoir and B. Vinter, Appl. Phys. Lett. **55**, 1859 (1989).
[15] P. J. Turley and S. W. Testsworth, J. Appl. Phys. **72**, 2356 (1992).
[16] P. J. Turley and S. W. Testsworth, Phys. Rev. B **44**, 3199 (1991); **44**, 8181 (1991); **44**, 12 956 (1991).
[17] K. W. Kim, A. R. Bhatt, M. A. Stroscio, P. J. Turley, and S. W. Testsworth, J. Appl. Phys. **72**, 2282 (1992).
[18] P. Orellana, F. Claro, E. Anda, and S. Makler, Phys. Rev. B **53**, 12 967 (1996).
[19] G. Kim, Dong-Wan Roh, and S. W. Paek, J. Appl. Phys. **81**, 7070 (1997).
[20] J. Chen, J. G. Chen, C. H. Yang, and R. A. Wilson, J. Appl. Phys. **70**, 3131 (1991).
[21] Y. Ando and T. Itoth, J. Appl. Phys. **61**, 1497 (1987).
[22] S. Adachi, J. Appl. Phys. **58**, R1 (1985).
[23] V. J. Goldman, D. C. Tsui, and J. E. Gunningham, Phys. Rev. B **36**, 7635 (1987).